Highly multiplexed profiling of single-cell effector functions reveals deep functional heterogeneity in response to pathogenic ligands

Yao Lu[a,1], Qiong Xue[a,1], Markus R. Eisele[a,b], Endah S. Sulistijo[a], Kara Brower[c], Lin Han[a], El-ad David Amir[d], Dana Pe'er[d], Kathryn Miller-Jensen[a,e,f,2], and Rong Fan[a,f,g,2]

[a]Department of Biomedical Engineering, Yale University, New Haven, CT 06520; [b]Institute for System Dynamics, University of Stuttgart, D-70563 Stuttgart, Germany; [c]IsoPlexis, New Haven, CT 06511; [d]Department of Biological Sciences, Columbia University, New York, NY 10027; [e]Department of Molecular, Cellular and Developmental Biology, Yale University, New Haven, CT 06520; [f]Yale Comprehensive Cancer Center, New Haven, CT 06520; and [g]Yale Stem Cell Center, Yale School of Medicine, New Haven, CT 06520

Edited by Garry P. Nolan, Stanford University, Stanford, CA, and accepted by the Editorial Board January 12, 2015 (received for review September 1, 2014)

Despite recent advances in single-cell genomic, transcriptional, and mass-cytometric profiling, it remains a challenge to collect highly multiplexed measurements of secreted proteins from single cells for comprehensive analysis of functional states. Herein, we combine spatial and spectral encoding with polydimethylsiloxane (PDMS) microchambers for codetection of 42 immune effector proteins secreted from single cells, representing the highest multiplexing recorded to date for a single-cell secretion assay. Using this platform to profile differentiated macrophages stimulated with lipopolysaccharide (LPS), the ligand of Toll-like receptor 4 (TLR4), reveals previously unobserved deep functional heterogeneity and varying levels of pathogenic activation. Uniquely protein profiling on the same single cells before and after LPS stimulation identified a role for macrophage inhibitory factor (MIF) to potentiate the activation of LPS-induced cytokine production. Advanced clustering analysis identified functional subsets including quiescent, polyfunctional fully activated, partially activated populations with different cytokine profiles. This population architecture is conserved throughout the cell activation process and prevails as it is extended to other TLR ligands and to primary macrophages derived from a healthy donor. This work demonstrates that the phenotypically similar cell population still exhibits a large degree of intrinsic heterogeneity at the functional and cell behavior level. This technology enables full-spectrum dissection of immune functional states in response to pathogenic or environmental stimulation, and opens opportunities to quantify deep functional heterogeneity for more comprehensive and accurate immune monitoring.

single-cell analysis | cytokine | immune effector function | cellular heterogeneity | Toll-like receptor activation

Emerging evidence indicates that cell-to-cell variability can give rise to phenotypic differences within a genetically identical cell population (1, 2). Nongenetic heterogeneity is also emerging as a potential barrier to effective therapeutic intervention (3, 4). Recent advances in single-cell molecular profiling are beginning to address these questions. Single-cell RNA sequencing revealed dynamic and bimodal gene expression (5). Single-cell multicolor flow cytometry (6) and mass cytometry (7) can quantify phenotypic diversity and differential drug response even across the hematopoietic continuum. Although a limited number of signaling proteins can be measured using intracellular staining, most of these technologies measure transcriptional or phenotypic marker expression in single cells. It remains an unmet need to directly measure cellular functional outcomes in a highly multiplexed manner and in single cells. In the immune system, the immune effector functions are largely mediated by a panel of effector proteins (e.g., cytokines and chemokines) secreted from single cells. Due to phenotypic plasticity and functional diversity, immune cells purified for a well-defined phenotype still display a wide range of effector functions in individual cells, but such deep functional heterogeneity has not been fully delineated due in part to the lack of technologies for quantifying all immune effector functions at the level of single cells.

Previously, multiplex profiling of effector proteins in single cells was limited (less than or equal to four) because of spectral overlap, for example, in a FLUOROSpot assay (8) or a nanowell-based microengraving assay (9). Multicolor flow-cytometric analysis with rigorous spectral compensation and mass cytometry extended the multiplexing capacity to 5–11 effector functions (7, 10). Recently, a spatial encoding mechanism that circumvents the limitation of spectral overlap was demonstrated for codetection of 15 proteins in single cells using highly miniaturized antibody microarrays placed in nanoliter cell-trapping chambers (11–13). However, this degree of multiplexing is still insufficient to dissect the full functional spectrum of a diverse range of immune cells.

Herein, we show simultaneous measurement of 42 effector proteins secreted from single immune cells, representing the highest multiplexing recorded to date for single-cell protein secretion assay. This was realized by combining spectral (color) and spatial (spots) multiplexing to drastically increase the number of proteins we can comeasure in single cells. We performed

Significance

We demonstrated codetection of 42 immune effector proteins in single cells, representing the highest multiplexing recorded to date for a single-cell secretion assay. Using this platform to profile differentiated macrophages stimulated with lipopolysaccharide reveals previously unobserved deep functional heterogeneity and varying levels of pathogenic activation, which is conserved throughout the cell activation process and prevails as it is extended to other Toll-like receptor (TLR) ligands and to primary human macrophages. The results indicate that the phenotypically similar cell population could still exhibit a large degree of intrinsic heterogeneity at the cell function level. This technology enables full-spectrum dissection of immune functional states in response to pathogenic stimulation and allows for more comprehensive and accurate monitoring of cellular immunity.

Author contributions: Y.L., K.M.-J., and R.F. designed research; Y.L., Q.X., E.S.S., K.B., and L.H. performed research; Y.L., Q.X., M.R.E., E.-a.D.A., D.P., K.M.-J., and R.F. analyzed data; and Y.L., K.M.-J., and R.F. wrote the paper.

Conflict of interest statement: R.F. and K.B. are cofounders of IsoPlexis, a company aiming to develop a microdevice product for single-cell immune function profiling.

This article is a PNAS Direct Submission. G.P.N. is a guest editor invited by the Editorial Board.

[1]Y.L. and Q.X. contributed equally to this work.

[2]To whom correspondence may be addressed. Email: rong.fan@yale.edu or Kathryn.miller-jensen@yale.edu.

This article contains supporting information online at www.pnas.org/lookup/suppl/doi:10.1073/pnas.1416756112/-/DCSupplemental.

a range of rigorous validation and comparative studies to fully establish the analytic metrics and the ability to quantify single-cell variability. Significantly, applying this platform to profiling phenotypically similar macrophages revealed previously unobserved deep functional heterogeneity and varying levels of pathogenic activation. It identified a subpopulation secreting macrophage inhibitory factor (MIF) that can potentiate the activation of LPS-regulated inflammatory cytokines. Advanced clustering analysis further identifies other functional subsets with distinct protein secretion profiles. The resultant population architecture is highly conserved throughout the cell activation process and as it is extended to other Toll-like receptor (TLR) ligands, suggesting the existence of an intrinsically heterogeneous response at the function level in a phenotypically similar population.

Results

Development and Characterization of a Single-Cell, 42-Plex Protein Secretion Assay. To detect proteins at the level of single cells, a subnanoliter microchamber array chip (3,080 or 5,044 microchambers per chip) fabricated in polydimethylsiloxane (PDMS) was used to isolate and trap individual cells to retain sufficient protein concentrations even if single cells were captured (Fig. 1*A* and *SI Appendix*, Fig. S1). The antibody barcode array slide was fabricated by flow patterning of 42 capture antibodies and three controls in 15 serpentine lines such that a set of immobilized antibodies, called an antibody barcode, comprises 15 isolated lines/bars and each contains three different antibodies. The width of one bar is 20 μm, and a full antibody barcode containing 15 bars spans ~900 μm. After seeding cells in the PDMS microchamber array, the antibody barcode slide is placed on top to seal the cells in isolated microchambers. Each microchamber contains at least a complete barcode to permit the codetection of a full panel of secreted proteins via a surface-bound immunesandwich assay using three-color detection (Fig. 1*A*). Compared with previous reports (11–15), this work for the first time (to our knowledge) combines spectral encoding (three colors) and spatial encoding (15 bars) to achieve an unprecedented degree of multiplexing (42 proteins and three positive controls) for single-cell protein secretion assay (Fig. 1*B* and *SI Appendix*, Fig. S2; the antibody and protein panel refers to *SI Appendix*, Tables S1 and S2). In this study, nonstimulated (basal) and stimulated macrophage cells were loaded into the assembled microchips, which were then imaged with a motorized phase contrast microscope to record the cell numbers and locations, followed by incubation for ~20 h to allow effector proteins to be secreted and bind to capture antibodies. Afterward, the antibody barcode array slide was removed and read out by introducing a mixture of all detection antibodies conjugated with fluorophores. A software suite has been developed for automated image analysis to count the number of cells in each microchamber and to quantify fluorescence intensities of the corresponding antibody barcode arrays. The data were analyzed using various computational tools to examine functional cellular heterogeneity and the correlation between individual functional subpopulations. Before conducting single-cell analysis, we completed rigorous validation experiments including spectral overlap and compensation, titration tests using recombinant proteins, and antibody cross-reactivity tests (*SI Appendix*, Figs. S3–S5) to establish analytical metrics and technical validity.

We used macrophage in response to LPS stimulation as a model system to investigate single-cell immune effector protein profiling (16–18). LPS activates the pathogen recognition pathway through binding to TLR4 and recapitulates the innate immune response against Gram-negative bacteria (19). LPS-stimulated macrophages are an ideal model system for single-cell secretion studies because (*i*) the signaling pathways are well characterized (20); (*ii*) a large number of effector proteins are expected to be secreted; and (*iii*) differentiated macrophages are postmitotic, and thus the influence

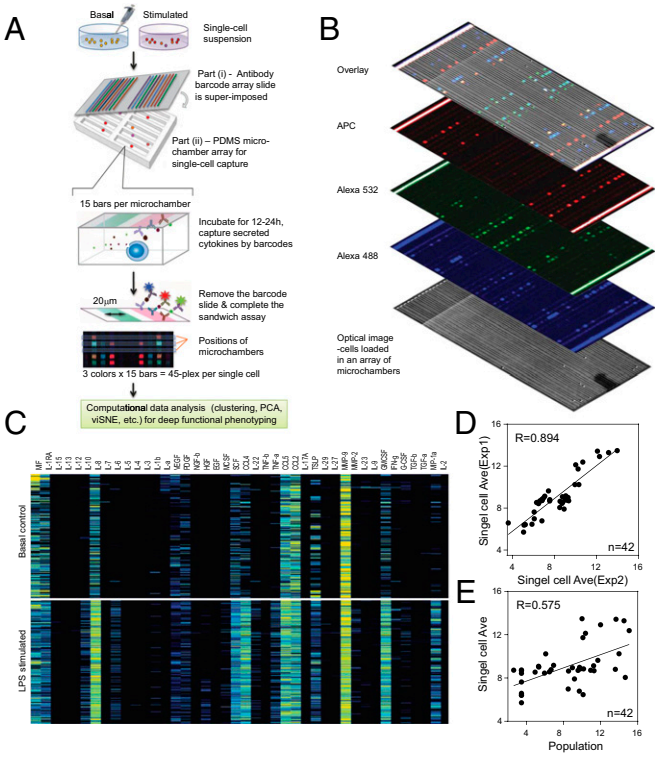

Fig. 1. Single-cell, 42-plex immune effector function profiling: workflow, data generation, and consistency test. (*A*) Workflow illustration of high-throughput profiling of single cells in basal and stimulated conditions for 42 secreted effector proteins. Optical photographs of the microchip and the microchamber array are shown in *SI Appendix*, Fig. S1. (*B*) Representative optical image showing a block of microchambers loaded with U937-derived macrophage cells and the corresponding scanned fluorescence images showing protein detection with three colors. The overlay of all these images is also shown. A large-scale scanned fluorescence images and the layout of 42 proteins in the three-color detection channels are shown in *SI Appendix*, Fig. S2. (*C*) Representative heat maps (basal vs. LPS stimulated) showing single-cell protein profiles measured on U937-derived macrophages, in which each row represents a complete protein profile from a single cell and each column is a protein of interest. (*D*) Correlation of protein secretion levels [*x*, *y* axes: log-scale arbitrary fluorescence unit (a.f.u.) + 1] between single-cell averages from two replicate microchip experiments. (*E*) Correlation of protein secretion levels (*x*, *y* axes: log-scale a.f.u. + 1) between single-cell average measured using microchips and population levels measured using conventional methods.

of cell cycle on functional heterogeneity is minimized. We started with macrophages derived from the human monocyte cell line U937 (*SI Appendix*, Fig. S6). The macrophage phenotype was confirmed by the expression of cluster of differentiation (CD)11b and CD14 (see flow cytometry analysis in *SI Appendix*, Fig. S7). A representative raw dataset from single-cell, 42-plex protein secretion profiling of basal (n = 666) and LPS-stimulated (n = 1,347) macrophages is shown as two heat maps, respectively (Fig. 1*C*, raw data without clustering). Each row of the heat map represents a single cell, and each column corresponds to a protein of interest. Two comparative experiments were conducted to validate the assay results. The first compares the secretion levels for an "average" single cell from two independent microchip assays of LPS-treated U937-derived macrophages. The two independent experiments show tight correlation (Pearson r = 0.89, P < 0.0001; Fig. 1*D*), indicating excellent consistency between single-cell microchip tests. The second compares secretion levels of all secreted proteins for an average single cell with the corresponding secretion from a cell population sample. There is a reasonable level of correlation

between average single-cell and cell population secretion profiles ($r = 0.57$, $P < 0.0001$; Fig. 1*E* and *SI Appendix*, Fig. S8) (5), despite significant differences in culture conditions between the two assays.

Data Quantification, Comparative Studies, and Validation Experiments. We compared basal and LPS-stimulated secretion following data normalization for the single cells assayed in the microchamber. An advantage of our microchip platform is the presence of zero-cell microchambers that can be used as an internal control to set the threshold of detection for each secreted protein. The fluorescence intensity shows distinct distribution between zero-cell and single-cell data, although the background signal for each protein varies substantially (data for four representative proteins shown in Fig. 2*A*). The intensity of the antibody barcodes in the microchambers with zero cells were analyzed and the threshold of detection for single-cell secretion was set as the mean intensity plus 2 × SD of the zero-cell wells, in a manner similar to the isotype control for flow cytometry. Overall, we reliably detected 33 out of 42 proteins above background level (Wilcoxon–Mann–Whitney test, $P < 0.05$; *SI Appendix*, Table S3). The threshold gate permits quantification of the fraction of cells positively secreting a given protein in a way similar to flow-cytometric data quantification (Fig. 2*B* and *SI Appendix*, Fig. S9). Ten proteins were significantly up-regulated by LPS stimulation according to a bootstrapping and Wilcoxon–Mann–Whitney test with $\alpha = 0.0012$ (*SI Appendix*, Table S3). Interestingly, although LPS is a potent activator of the proinflammatory response, all of the effector proteins measured in this study show fractional secretion with significant cell-to-cell heterogeneity. We found that, in most cases, up-regulation of protein secretion upon LPS stimulation could be attributed to both an increase in the fraction of secreting cells and the secretion intensity from those cells [e.g., TNFα, IL-6, chemokine C–C motif ligand (CCL)3/macrophage inflammatory protein (MIP)-1α, and CCL4/MIP-1β]. However, in some cases, only the fraction increased (e.g., IL-8), or only the secretion intensity increased (e.g., CCL5/RANTES). Interestingly, proteins such as IL-6 that are strongly induced by LPS stimulation in the cell population show fractional bimodal secretion with significant cell-to-cell heterogeneity in single cells, consistent with other recent reports of LPS-stimulated IL-6 activation in monocytic cells (5). Notably, macrophage migration inhibitory factor (MIF), which is involved in LPS-mediated proinflammatory responses (21–23), is secreted from a significant fraction of cells in the basal state and remains largely unchanged upon LPS treatment.

We then compared our results to flow-cytometric analysis of intracellular cytokine staining (ICS) performed on 12 proteins that represent a range of protein secretion levels measured in the single-cell microchips (*SI Appendix*, Fig. S10, and select scatter plots shown in Fig. 2*C*). Our approach often identified a smaller fraction of cytokine-secreting cells compared with ICS, which is in accordance with previous reports (24–26). This is due to a number of reasons, one of which is the biological difference between two assays: our method measures actual secretion of single cells, whereas ICS requires the use of vesicle transport inhibitors to block secretion and retain synthesized proteins in the cells for flow-cytometric analysis. However, the increase in the fraction of cells that respond to LPS stimulation is well correlated between the two methods (Pearson $r = 0.87$; $P = 0.2658$ in paired t test; Fig. 2*D*).

We further conducted a range of validation experiments to confirm that (*i*) cells captured in microchambers and incubated for 20 h remain viable (*SI Appendix*, Fig. S11); (*ii*) cells did not experience hypoxia, confirming that PDMS, a gas-permeable elastomer, effectively maintains oxygen levels in the microchambers (*SI Appendix*, Fig. S12); and (*iii*) the protein secretion profile is not altered by the PDMS surface compared with conventional cell tissue culture plates (*SI Appendix*, Fig. S13).

Single-Cell Analysis Reveals a Temporal "Anticorrelation" Between MIF and LPS-Regulated Cytokines. To facilitate visualization of our highly multidimensional dataset, we used principal component analysis (PCA), a technique that reduces the dimensionality of the data by identifying new axes (principal components or PCs) that capture maximal covariation in the data (27, 28). PCA has recently been used to interpret other single-cell datasets resulting from high-dimensional assays such as mass cytometry (7, 29). We reduced our dataset to those proteins that were detected above background in three independent experiments (25 proteins; *SI Appendix*, Table S3). We found that PC1 (accounting for 25% of the total variation) separated some of the

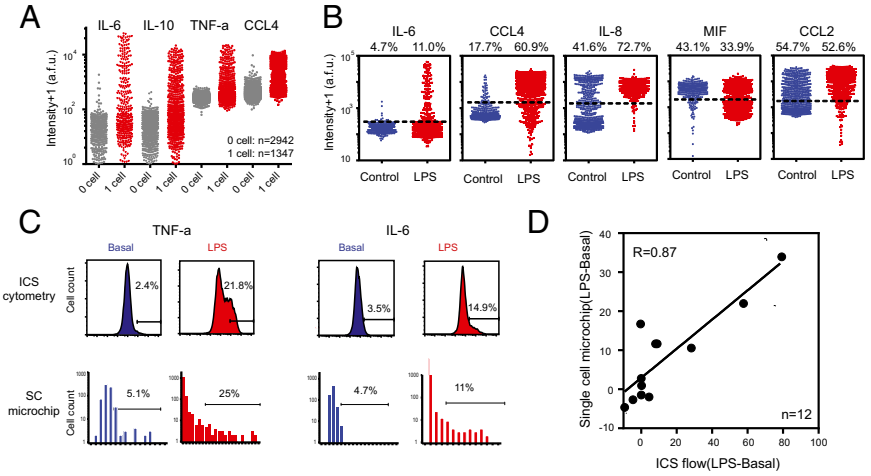

Fig. 2. Data quantification and comparison with ICS flow cytometry. (*A*) Vertical scatter plots showing fluorescence intensity detected for four proteins in zero-cell (black dots) and single-cell (red dots) microchambers. The zero-cell microchamber data serve as an internal control; the average plus 2SD of the zero-cell data are used to gate single-cell protein secretion in a way similar to flow cytometry data analysis. (*B*) Vertical scatter plots comparing single-cell protein secretion at the basal level (blue dots) and upon LPS stimulation (red dots). The dashed line marks the gate defined as (zero-cell data average plus 2SD). The data were shifted vertically to match the gates obtained from two microchips. (*C*) Histograms showing single-cell protein secretion measured by microchip or flow cytometry for two representative proteins (TNFα and IL-6). (*D*) Comparison between single-cell microchip and flow cytometry ICS for all 12 proteins (*SI Appendix*, Fig. S10). The correlation plot shows the change of protein secretion frequency induced by LPS relative to basal state.

LPS-treated cells from unstimulated cells (Fig. 3*A*). Consistent with this observation, the proteins that defined PC1 were enriched for proteins that are positively regulated by LPS (Fig. 3*B*). Interestingly, a significant fraction of LPS-stimulated cells were indistinguishable from the basal state, suggesting that some cells were refractory to LPS stimulation. In contrast, both unstimulated and LPS-treated cells separated along PC2 (11% of the total variation), which appeared to be influenced by the secretion level of MIF (Fig. 3 *A* and *B*). We further observed that MIF was anticorrelated with LPS activation (Fig. 3*B* and *SI Appendix*, Fig. S14). To confirm this, we calculated the conditional probability of secretion of LPS-activated cytokines for MIF^+ and MIF^- cells and found that MIF^+ cells were significantly less likely to secrete IL-8, CCL3, CCL4, IL-6, and IL-10 compared with MIF^- cells (Fig. 3*C*).

Although this finding suggests that MIF is antagonistic to inflammation, previous literature has confirmed a proinflammatory role for MIF in innate immune activation (21, 22). MIF is produced constitutively in the differentiated U937 macrophage population as measured in both single-cell and cell population assays. We hypothesized that this discrepancy might be due to timing and differential response of MIF-secreting cells. To test this, we took advantage of our platform to measure the secretion from live cells isolated in defined locations to track the change of all proteins secreted from the same single cells before and after LPS stimulation. Briefly, after measuring secretion from unstimulated macrophages for 6 h, we removed the antibody barcode slide that detected the basal secretion profile, added LPS to the single-cell capture chip, and then replaced a new barcode slide to measure protein secretion from the same single cells upon LPS stimulation (Fig. 3*D*). Using these data, we investigated how MIF secretion in the basal state affects the secretion of other factors upon LPS stimulation.

We observed that ∼10% of basal cells were positive for MIF secretion, all of which were negative for MIF secretion following LPS stimulation (green in Fig. 3*E*). Similarly, cells positive for MIF secretion following LPS stimulation were negative for MIF secretion in the basal state (black in Fig. 3*E*). These data suggest that individual cells release MIF for relatively short periods of time. Importantly, cells that were MIF^+ in the basal state demonstrated an increased probability of secreting CCL4 and at higher levels compared with the cells that were positive for MIF following LPS stimulation (Fig. 3*F*). Overall, cells positive for MIF secretion in the basal state have a higher probability of LPS-induced IL-8, CCL4, TNF, and IL-10 secretion than cells that do not secrete MIF before LPS activation (Fig. 3*G*). Thus, our results indicate a differential response of $MIF^{+/-}$ cells to LPS stimulation and suggest that MIF release either directly potentiates activation by LPS or is indicative of a potentiated state. This explains the apparent discrepancy of anticorrelation between MIF and other cytokines in single-cell data and is consistent with a proinflammatory role for MIF in the LPS response (21, 22).

Clustering High-Dimensional Single-Cell Data Reveal Conserved Subpopulations in Response to TLR Ligands. Although PCA identified important functional relationships between cytokines, it

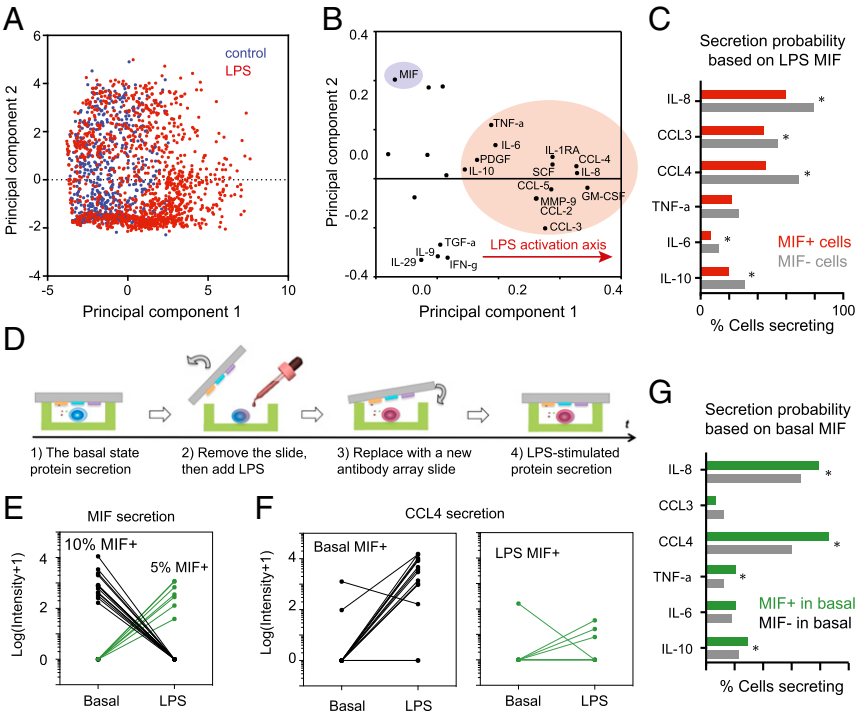

Fig. 3. Single-cell analysis implies an anticorrelation relationship between MIF and LPS-regulated cytokines. (*A*) Principal component analysis (PCA) indicates a major shift toward the functional state dictated by principal component 1 (PC1) upon LPS stimulation. U937-derived macrophage cells were measured. Blue: basal or nonstimulated cells. Red: LPS-stimulated cells. (*B*) PCA plot showing the contribution of individual proteins to PC1 and PC2. LPS-induced proinflammatory cytokines constitute to the major portion of PC1. MIF is uniquely associated with PC2. (*C*) Comparing secretion probability of LPS-regulated cytokines between MIF^+ and MIF^- subpopulations. Measurement of the same single cells before and after stimulation reveals a unique role for MIF to potentiate the activation of LPS-regulated cytokine functions. (*D*) Schematic illustration of the procedure for measuring the secretion of all 42 proteins from the same single cell before and after LPS stimulation. (*E*) Change of MIF secretion function in the same single cells before and after LPS stimulation. It shows MIF-secreting cells in the beginning all become MIF-negative after LPS stimulation. The cells that secrete MIF after LPS stimulation did not produce MIF before stimulation. Each straight line corresponds to the protein level change in a same single cell. (*F*) Relation between MIF-secreting cells and CCL4 secretion. MIF secretion in the basal state is associated with increased probability and the level of CCL4 secretion following LPS stimulation. (*G*) Probability of secreting LPS-regulated cytokines after stimulation in relation with MIF secretion at the basal level. Asterisk indicates $P < 0.05$ by Wilcoxon–Mann–Whitney test.

failed to distinguish clear boundaries separating activated and quiescent cell populations (Fig. 3*A*). We therefore exploited a high-dimensional data analysis tool, viSNE (30), to visualize the deep functional phenotypes in response to stimulation. viSNE, which is based on the t-Distributed Stochastic Neighbor Embedding algorithm (31), projects high-plex single-cell data to a 2D space to visualize cell subpopulations, and it has shown improved segregation of subpopulations compared with PCA (30). Here, we further investigated single-cell cytokine functions in response to other TLR ligands, including the TLR1/2 ligand PAM3CSK4 (PAM), and the TLR3 ligand polyinosine-polycytidylic acid [poly(I:C)]. All single cells from four treatment conditions [basal, PAM, poly(I:C), and LPS] were mapped onto the same dimensions using viSNE, revealing five loosely defined subpopulations (Fig. 4 *A* and *B*, and *SI Appendix*, Fig. S15): a MIF-specific population (MIF$^+$), a quiescent cell (QC) subpopulation that produce few cytokines, a polyfunctional fully activated (PFA) population that produce most LPS-regulated cytokines at high levels, and two partially activated (PA) subpopulations distinguished by CCL2 secretion. PA-high corresponds to the cells producing both matrix metalloprotease 9 (MMP9) and CCL2, whereas PA-low cells produce MMP9 but not CCL2 (for all cytokine functions, refer to *SI Appendix*, Fig. S16). LPS stimulation substantially increased the polyfunctional subpopulation and the covariation between proteins (*SI Appendix*, Figs. S17 and S18), which is the most noticeable response, yet still represents only a fraction of all macrophage cells examined. IL-8 secretion defines the polyfunctional subpopulation in both basal and stimulated conditions (Fig. 4*B*). Interestingly, viSNE unambiguously identified a MIF-secreting subpopulation,

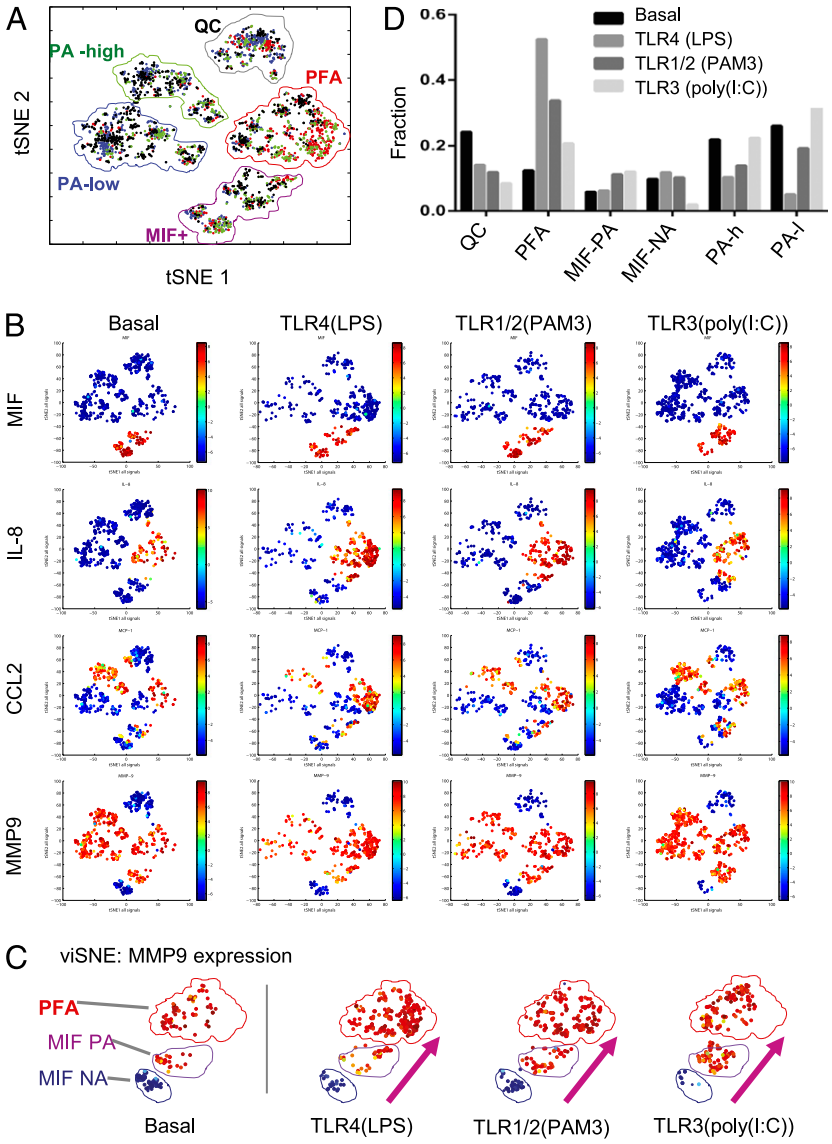

Fig. 4. Functional heterogeneity and subpopulations of U937-derived macrophages in response to TLR ligands. (*A*) viSNE analysis reveals multiple clusters (functional subpopulations) emerging consistently in response to three TLR ligands. They can be classified as quiescent cell (QC), polyfunctional fully activated (PFA), partially activated (PA)-high, PA-low, and MIF-secreting (MIF$^+$) populations, respectively (*SI Appendix*, Fig. S15). Each dot is a single cell under different treatment conditions: basal (blue), LPS (red), PAM3 (green), and poly(I:C) (black). (*B*) Distribution of individual proteins (MIF, IL-8, CCL2/MCP-1, MMP9) in viSNE plots for different conditions (basal, TLR4, TLR1/2, TLR3 activated) (see viSNE for all proteins in *SI Appendix*, Fig. S16). (*C*) Close view of the functional phenotype shift within a MIF$^+$ population. According to the coexpression of MMP9, MIF-secreting cells can be subdivided to a MIF partially activated (MIF PA) and a MIF nonactivated (MIF NA) population. (*D*) Quantification of all subpopulations in basal and stimulated conditions.

which is distinct and remains at a relatively unchanged frequency upon LPS stimulation. However, we observed that the MIF-positive basal cells became negative for MIF secretion and positive for IL-8 secretion upon LPS stimulation. The MIF-positive population in a LPS-stimulated sample is replenished from the cells originating in other subpopulations in the basal state, suggesting the existence of phenotypic homeostasis for MIF production among all functional cell subsets, which was never observed previously.

We next considered how LPS, PAM3, and poly(I:C) specifically modulated the fraction of cells in each of these functional groups. Overall, LPS induced a more potent response than either PAM3 or poly(I:C), resulting in a greater fraction of PFA cells [53% for LPS vs. 34% for PAM3 and 22% for poly(I:C)]. Within the PFA population, LPS induced a larger subset of PFA cells to secrete IL-6 and IL-10 compared with PAM3. Poly(I:C) appears to be the least potent ligand, with minimal increase of PFA population, although this could be due to the fact that our antibody panel did not include a large number of antiviral effectors. However, we noticed a significant phenotypic shift of MIF-secreting cells upon stimulation with poly(I:C) (Fig. 4 *C* and *D*). MIF^+ cells are divided into two subsets, namely MIF partially activated (MIF PA) and MIF nonactivated (MIF-NA), defined by the ability to cosecrete MMP9. Although the total number of MIF^+ cells remained relatively constant (~16–21%), PAM3 and poly(I:C) markedly increased the MIF PA fraction. In particular, poly(I:C) induced a marked up-conversion of MIF NA to MIF PA. Interestingly, although poly(I:C) is less potent in producing PFA cells, it is the most effective in activating quiescent cells and resulted in substantial increase of PA populations. Taken together, these results unambiguously show highly conserved heterogeneous population structures in response to TLR ligands (*SI Appendix*, Figs. S19 and S20).

Single-Cell Analysis of Primary Monocyte-Derived Macrophage Cells. We further conducted single-cell protein secretion profiling on primary macrophages derived from a healthy donor. Human monocytes were isolated, induced to differentiate into an M1-like phenotype (32), and then studied for their single-cell secretion response to all three TLR ligands. The results showed that the primary cells also gave rise to highly structured, tiered responses. Overall, there are more cell subpopulations/clusters, which is expected in that the primary macrophage cells are more heterogeneous than the cell line-derived macrophages. However, we were still able to identify cell subpopulations using viSNE with characteristics that were similar to the macrophage cell line (Fig. 5*A* and *SI Appendix*, Figs. S21 and S22): the PFA population with most polyfunctional cells, the PA-high population with multiple cytokines secreted including MMP9, three PA-low populations with limited cytokines secreted including MMP9, and a quiescent population. All together, these subpopulations account for >80% of the entire cell population. Three new subpopulations (N1, N2, N3) were observed in this sample. N1 is proinflammatory population secreting TNFα and IL-6. N2 is an IL-1 receptor antagonist (IL-1RA)-secreting population, and N3 is relatively quiescent. The changes of all subpopulations in response to different TLR ligands are summarized in Fig. 5*B*. Interestingly, although MIF secretion is relatively rare in this primary macrophage sample, viSNE unambiguously identified a cluster of MIF-secreting cells, which is distinct from other populations. Upon LPS stimulation, the MIF-positive subpopulation, although relatively small, remains largely unchanged, which is consistent with the result from U937-derived macrophages. A closer view of the PFA population reveals that it can be divided into a more polyfunctional subset (e.g., $IL\text{-}8^+/CCL4^+$) and a less polyfunctional subset ($IL\text{-}8^+/CCL4^-$) (Fig. 5*C*). Quantification of these two subsets indicates LPS induces most abundant $IL\text{-}8^+/CCL4^+$ PFA cells, whereas poly(I:C) is least effective in term of inducing the formation of $IL\text{-}8^+/CCL4^-$ cells (Fig. 5*D*), similar to the U937-derived macrophage cells. The phenotypic shift in all three TLR stimulations follows a conserved heterogeneous population architecture.

Discussion

We developed a microchip technology that, for the first time (to our knowledge), demonstrated highly multiplexed (40+) profiling

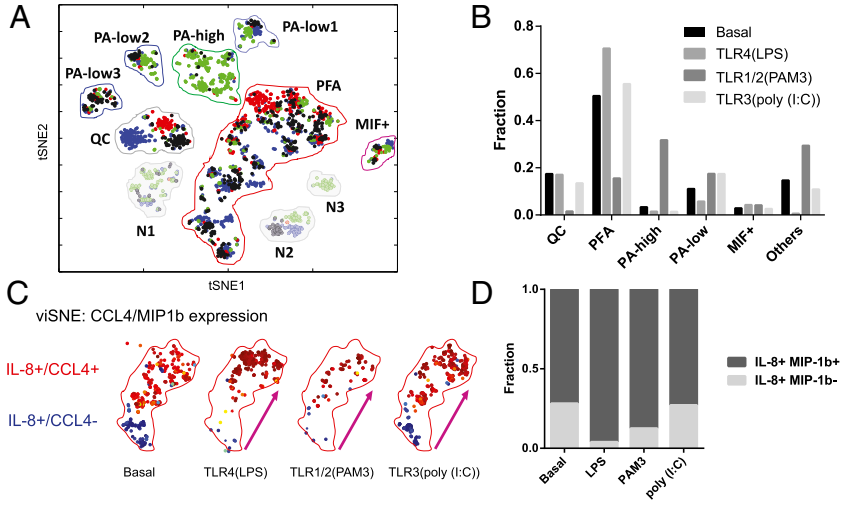

Fig. 5. Functional heterogeneity and subpopulations of primary human monocyte-derived macrophages in response to TLR ligands. (*A*) viSNE analysis reveals multiple clusters (functional subpopulations) emerging consistently in response to three TLR ligands [LPS, PAM3, and poly(I:C)]. They can be classified as quiescent cell (QC), polyfunctional fully activated (PFA), partially activated (PA)-high, PA-low, and MIF-secreting (MIF^+) populations, respectively (*SI Appendix*, Fig. S21). Each dot is a single cell under different treatment conditions: basal (blue), LPS (red), PAM3 (green), and poly(I:C) (black). (*B*) Quantification of all subpopulations in basal and stimulated conditions (*SI Appendix*, Fig. S22). (*C*) Enlarged view of the PFA population indicates a phenotypic shift from a relatively less polyfunctional (e.g., $IL\text{-}8^+/CCL4^-$) to more polyfunctional (e.g., $IL\text{-}8^+/CCL4^+$) phenotype upon stimulation. (*D*) Quantification of $IL\text{-}8^+/CCL4^-$ and $IL\text{-}8^+/CCL4^+$ cells within the PFA population in response to TLR ligands. Similarly, LPS is the strongest activator and poly(I:C) induced minimal increase of the $IL\text{-}8^+/CCL4^+$ functional subset.

of immune effector function proteins at the level of single cells. Applying this technology to the study of phenotypically similar macrophages has generated previously unidentified insights to understanding immune cell functional states and response to pathogenic stimulation. First, it reveals the existence of a dynamic macrostructure within the macrophage cell population, and this structure is conserved in response to different TLR stimulation. Second, we observed distinct deep functional subpopulations with varying levels of activation and differential responses in a phenotypically pure cell population. Third, specifically, we identified a MIF-secreting subpopulation that potentiates the activation of LPS-induced cytokine function. These findings demonstrate the power of single-cell high-plex protein secretion profiling for deep functional phenotyping and comprehensive dissection of immune functional states of single cells. Upon further improvement of cell adhesion in microchambers, our microchip technology has the potential to track single-cell protein secretion dynamics, which can add another axis to better differentiate functional subpopulations and identify phenotypic changes upon stimulation.

The current technology is designed for in-depth functional analysis of phenotypically "pure" populations. It is well suited to measuring small numbers of cells (~1,000) separated by fluorescence-activated or magnetically assisted cell sorting based upon surface markers. To further expand the utility of this technology to unsorted populations, it is feasible to conduct immunofluorescence staining for phenotypic surface markers before loading cells into microchip and then conduct fluorescence imaging to identify phenotype. Similar to other nanowell-based technologies (9), our microchip isolates individual cells in microchambers and eliminates the effect of paracrine signaling. Although it is also believed that this type of assay can better measure the intrinsic secretion function of individual cells without the complication by the secondary activation induced by paracrine, one must be aware of the difference between single-cell secretion and the bulk secretion that may not always give the same protein profile. Interestingly, the presence of multicell microchambers in our microchip offers a different route to investigate the role of paracrine signaling in modulating collective responses as exemplified by recent studies (33, 34), which is a unique feature of this technology compared with flow cytometry. In this work, we have demonstrated the culture of both cell line-derived and primary macrophage cells in microchip over a period of 20 h. The ability to conduct a longer time course study is yet to be evaluated.

Nevertheless, to the best of our knowledge, this technology represents the most informative tool to date for profiling the immune effector functions in single cells (35). It can be widely applied to delineating functional states of other immune cells (e.g., T lymphocytes and dendritic cells) or even nonimmune cells (e.g., beta cells and epithelial tumor cells). It is inexpensive, reliable, and quantitative, requiring minimal input of cells, and thus may have tremendous potential for widespread applications including comprehensive immune monitoring in both preclinical and clinical applications (36–38).

Materials and Methods

Fabrication of Antibody Barcode Arrays. The mold for the antibody barcode in-house manufacturing (flow patterning) PDMS replica is a silicon master etched with the deep reactive-ion etching (DRIE) method. It was pretreated with trimethylchlorosilane (TMCS) (Aldrich) vapor overnight to facilitate PDMS release. PDMS prepolymer elastomer base and curing agent (RTV615; Momentive) was mixed completely (parts A and B in 10:1 ratio) and poured onto the silicon master. Air bubbles were removed via a vacuum desiccator for 1 h, and the PDMS on mold was cured in the oven at 80 °C for 2 h. After curing, the PDMS layer was peeled off the mold and holes for inlet and outlet ports were punched. Each flow-patterning PDMS chip measures 75 mm (length) × 25 mm (width), the size of a glass slide, and 6 mm in height. The device was cleaned via sonication in 70% (vol/vol) ethanol and 2-propanol before bonding with a poly-L-lysine microarray slide (Erie Scientific). The assembly was then baked in the oven at 80 °C for 2 h to strengthen the bonding. The PDMS microchip for antibody flow patterning contains 20 separate microchannels arranged in a serpentine pattern across chip that can pattern up to 20 different solutions, respectively. The typical width and pitch of antibody within the barcode are 20 and 50 μm, respectively, in the PDMS flow-patterning microchip. A full antibody barcode set of all 20 antibodies measures 900 μm.

For the flow patterning of the antibody barcodes, 2 μL of different antibody mixtures (*SI Appendix*, Table S1 and Fig. S1) were injected into microchannels separately and flowed through the microfluidic channels until dry (~12 h) with forced N_2 at 2 psi. For spectral encoding, the antibody mixture contained a mixture of three antibodies at 0.5 mg/mL in 1× PBS in each per channel. All of the antibodies used in experiments are summarized in *SI Appendix*, Table S1. Through flow patterning, antibodies are immobilized on the poly-L-lysine glass slide to form the antibody barcode. After flow patterning, PDMS layer was released and the glass slide was blocked with 3% BSA (Sigma). After blocking, the glass slide was rinsed with 1× PBS and deionized (DI) water for desalination and gently blown dry with forced N_2. Functionalized barcode slides were in the refrigerator at 4 °C until use (<1 wk).

Fabrication of Microchamber Array Chips. The mold for the 3,000+ subnanoliter microchamber array is a silicon master etched with the DRIE method. It was also pretreated with TMCS (Aldrich) vapor overnight to facilitate PDMS release. The microfluidic chamber array chips for single-cell capture were fabricated from PDMS (RTV615; Momentive; parts A and B in 10:1 ratio) using standard soft lithography techniques as described above. Air bubbles were removed via vacuum desiccator for 1 h, and the PDMS was cured in the oven at 80 °C for 2 h. Resultant chips after PDMS removal from the mold were 25 mm (width) and 35 mm (length). Each array contains 14 columns of 220 microwells (totaling 3,080 wells for cell capture). Each microwell measures 35 μm (width) × 1,850 μm (length) × 35 μm (depth) with 35-μm spacing to optimize signal cell capture and interface with two full antibody barcode sets.

Conjugation of Detection Antibodies with Fluorophores. The 488 group and 532 detection antibodies were conjugated before use with Alexa Fluor 488 and Alexa Fluor 532 dyes, respectively, following the protocol provided by the supplier (Invitrogen). The 635-nm allophycocyanin (APC) detection was achieved by an on-chip subsequent incubation step described below. For this group, biotinylated antibodies were added to the detection antibody mixture without conjugated fluorophores.

Cell Culture and Stimulation. Human U937 cell line was purchased from American Type Culture Collection (ATCC) and cultured in RPMI medium 1640 (Gibco; Invitrogen) supplemented with 10% FBS (ATCC). The U937 cells were differentiated with 50 ng/mL phorbol 12-myristate 13-acetate (PMA) (Fisher) for 48 h, followed by culture in fresh standard medium for 24 h. The cells were harvested with trypsin for single-cell experiments. The cells were challenged with 100 ng/mL LPS (Calbiochem) just before the suspension was pipetted onto PDMS microwell array. LPS (100 ng/mL), Pam3 (250 ng/mL), and poly(I:C) (10 μg/mL) from InvivoGen were used to compare cell response to different TLR ligands. Human PBMCs were isolated from buffy coat (Research Blood Components) using Ficoll-paque (GE Healthcare). Monocytes were further isolated from PBMC using a pan monocyte isolation kit (Miltenyi Biotec) and differentiated into macrophages by first culturing cells with RPMI complete medium (RPMI containing 20% heat-inactive FBS, 1% penicillin/strep, and 2 mM L-glutamine) containing GM-CSF (50 ng/mL; R&D) for 3 d and then RPMI complete medium for 4 d.

Single-Cell Multiplex Protein Secretion Assay. Before performing the single-cell trapping experiment, the PDMS microwell array was blocked with 3% BSA solution (Sigma) for 2 h and then rinsed with fresh cell medium. Cells were suspended in fresh medium just before cell capture to a working concentration of 0.4 million cells per mL, optimal for single-cell capture. Stimulants as described above were added. The PDMS microwell array was placed facing upward, and cell culture media solution (from rinsing) was removed until a thin layer remained on the PDMS microwell array surface. Cell suspension was pipetted (250 μL) onto the microwell array and allowed to settle for 10 min so that cells would fall into the microwells. The antibody glass slide was put on top of the PDMS microwell array with the antibody barcode resting face-down on the cell capture chambers. Subsequently, the PDMS microwell array and glass slide were clamped tightly with screws using a custom polycarbonate plate clamping system. Single cells were trapped in the microwell array and cell counts were confirmed by an imaging sequence described below. The microchip assembly was placed in a standard 5% CO_2

incubator at 37 °C during the period of cell secretion. After ~20 h, the microchip assembly was dissembled and the antibody barcode slide was removed and rinsed with 3% BSA. The antibody barcode glass slide was developed for 1 h at room temperature by introducing a mixture of fluorophore-labeled detection antibodies (blue and green channels) and biotinylated detection antibodies (red channel). The detection antibody mixture consists of the detection antibodies (*SI Appendix*, Table S1) at 0.25 μg/mL each in 1:200 suspension in 3% BSA. Following this step, the barcode slide was rinsed with 3% BSA solution. The 250 μL of 1:100 suspension APC dye-labeled streptavidin (eBioscience; 5 μg/mL) were added onto glass slide to detect the 635-nm detection antibody group, and the barcode slide was incubated for another 30 min. Afterward, the glass slide was washed with 3% BSA again and then blocked with 3% BSA for 30 min. Following the BSA blocking, the glass slide was dipped in Dulbecco's PBS (DPBS), DPBS, DI water, DI water sequentially, and gently blown dry with forced N_2 gas.

Finally, the antibody barcode array slide was rinsed with 1× PBS, 0.5× PBS, and DI water sequentially, dried with forced N_2 gas, and then scanned with a four-laser microarray scanner (Molecular Devices; Genepix 4200A) for protein signal detection. Microwell array images with cell counts were subsequently matched to their protein signals by well and by antibody for further data analysis.

Imaging and Counting of Cells. The assembly was imaged before incubation on Nikon Eclipse Ti microscope with an automatic microscope stage to acquire optical images (both dark-field and oblique view) of the microwell array, which provides information on the number and location of cells within each microwell. The oblique view is a custom half-moon optical filter used to provide shadow on spherical objects to make cell detection easier. The dark-field image of the microwell array was used to define the location and spatial identity of each microchamber, and the oblique image was used to define the cell numbers and their locations. Both images can be processed in Nikon software (NIS-Elements Ar Microscope Imaging Software) by defining threshold on each image to realize automated cell counting. The cell counts will then be matched with the extracted fluorescent data to their respective cell chambers as described further in *Image Processing and Quantification*.

Population Antibody Microarray. The cell population assay was performed on custom-printed antibody microarray, which was spotted with a Spotbot 3 microarrayer (Arrayit) on poly-L-lysine glass slides. Twelve identical subgroups that had the same antibody pattern were printed on each glass slide (each antibody spot was <1 mm). After printing, the antibody glass side was kept in a wet box (containing saturated NaCl solution at 75% relative humidity) for 5 h. Before cell population assay, the glass side was bonded with a custom 12-hole PDMS microwell slab (each hole at $D = 1$ cm) and blocked with 3% BSA solution for 2 h. Cell culture supernatant was added into different microwells for each sample and allowed to incubate for 1 h. Following incubation, ELISA immunoassay procedures were performed, and the results were detected and analyzed with Genepix scanner and software.

ICS. Cells are harvested and seeded into tissue culture Petri dish in 10^6/mL density with both control and treated cells. After 2 h, the secretion inhibitor brefeldin A (Biolegend) was added. The cells were then incubated for 22 h before harvested for intracellular flow cytometry. Cell fixation and intracellular staining were performed according the manufacturer's protocol (Cell Signaling). BD Accuri C6 flow cytometer was used to collect and analyze data.

Fluorescence Imaging and Analysis. Genepix 4200A scanners (Molecular Devices) were used to obtain scanned fluorescent images. Three color channels, 488 (blue), 532 (green), and 635 (red), were used to collect fluorescence signals. The image was analyzed with GenePix Pro software (Molecular Devices) by loading and aligning the microwell array template followed by extraction of fluorescence intensity values per antibody per microwell. Fluorescence results were extracted with the image analysis tool in GenePix Pro. The fluorescence results were then matched to each of the 3,080 chambers of the subnanoliter microchamber array for cell counts and cell location as previously extracted from the optical imaging steps.

Image Processing and Quantification. Cell counts and microwell spatial information were extracted from the dark-field and oblique optical images of the microwell array by Nikon Elements software (Nikon Imaging Solutions). The microwell spatial information and the definition of each microwell boundary were gained by manually adjusting the edge detection threshold using the binary editor feature of the software. Microwell boundaries were confirmed vs. the mask design with 220 microwells per column and 14 columns per chip. Cell counting was achieved using the binary editor feature tool of the software to manually count each spherical cell in the oblique view. Subsequently, a fully automated C++/QT QML software was developed to perform this function and confirm cell counts (DETECT; IsoPlexis). Protein signal data were extracted from the multicolor fluorescent images using GenePix Pro-6.1 (Molecular Devices) by aligning a microwell array template with feature blocks per antibody per microwell to the protein signal features. Data were extracted using the image analysis tool to gain the mean photon counts per protein signal bar (i.e., 20 antibodies per barcode) per microwell and match to the cell counts from the microwell array.

Data Analysis and Statistics. After Genepix Pro data extraction per feature per microwell, the resultant data matrix consisted of mean photon counts (PCs) per each protein signal feature, which was a $42 \times 3{,}080$ array of 42 proteins measured per 3,080 microwells. These microwells, based on their spatial location, were matched to their cell counts and cell locations, organizing the 3,080 microwell measurements into 0, 1, 2, 3, 4+ cell wells with associated protein signals. Each signal underwent background subtraction to determine the PCs from true antigen binding events (compared with noise). Zero-cell wells and their associated protein signals were used as on-chip controls to provide a measure of local antibody-specific background and were averaged across region on chip. The mean of the zero-cell wells per antibody plus $2D$ (defined here as an activity threshold or "gate") was subtracted from each 1, 2, 3, 4+ cell well per antibody. Typical thresholds were on the order of 200–700 PCs, below the calculated limit of detection. Global nonspecific background, calculated from a feature on chip outside the microwell, was also subtracted from each signal (typically 0–60 PCs). Postthreshold subtraction for visualization graphical formats, negative values were zeroed, and the data were log transformed using Log $(x + 1)$. A home-developed Matlab (MathWorks) code was created for automated extraction of fluorescent data and generation of scatterplots. Excel (Microsoft) and OriginPro 8 (OriginLab) were used to compile extracted data. A custom Python script was developed to automate data analysis. Statistical analysis, heat maps, hierarchical clustering, and PCA were performed in Matlab.

ACKNOWLEDGMENTS. We thank Sean McCuster at IsoPlexis for help in graphic analysis and design. We also acknowledge the Yale Institute for Nanoscience and Quantum Engineering and the Yale Nanofabrication Center for allowing us to use their facilities. This study was supported by NIH Library of Integrated Network-Based Signatures Program Technology Center Grant NIH U01 CA164252 (to R.F. and K.M.-J.), the Dana Farber Physical Sciences Oncology Center–Single Cell Profiling Core (NIH U54 CA143798 subaward) (to R.F.), National Cancer Institute Howard Temin Pathway to Independence Award NIH R00 CA136759 (to R.F.), National Science Foundation CAREER Award MCB-1149728 (to D.P), and NIH Grant R01CA164729 (to D.P.).

1. Altschuler SJ, Wu LF (2010) Cellular heterogeneity: Do differences make a difference? *Cell* 141(4):559–563.
2. Niepel M, Spencer SL, Sorger PK (2009) Non-genetic cell-to-cell variability and the consequences for pharmacology. *Curr Opin Chem Biol* 13(5-6):556–561.
3. Gascoigne KE, Taylor SS (2008) Cancer cells display profound intra- and interline variation following prolonged exposure to antimitotic drugs. *Cancer Cell* 14(2): 111–122.
4. Cohen AA, et al. (2008) Dynamic proteomics of individual cancer cells in response to a drug. *Science* 322(5907):1511–1516.
5. Shalek AK, et al. (2013) Single-cell transcriptomics reveals bimodality in expression and splicing in immune cells. *Nature* 498(7453):236–240.
6. Seder RA, Darrah PA, Roederer M (2008) T-cell quality in memory and protection: Implications for vaccine design. *Nat Rev Immunol* 8(4):247–258.
7. Bendall SC, et al. (2011) Single-cell mass cytometry of differential immune and drug responses across a human hematopoietic continuum. *Science* 332(6030):687–696.
8. Ahlborg N, Axelsson B (2012) Dual- and triple-color fluorospot. *Methods Mol Biol* 792: 77–85.
9. Bradshaw EM, et al. (2008) Concurrent detection of secreted products from human lymphocytes by microengraving: Cytokines and antigen-reactive antibodies. *Clin Immunol* 129(1):10–18.
10. De Rosa SC, Herzenberg LA, Herzenberg LA, Roederer M (2001) 11-color, 13-parameter flow cytometry: Identification of human naive T cells by phenotype, function, and T-cell receptor diversity. *Nat Med* 7(2):245–248.
11. Fan R, et al. (2008) Integrated barcode chips for rapid, multiplexed analysis of proteins in microliter quantities of blood. *Nat Biotechnol* 26(12):1373–1378.
12. Ma C, et al. (2011) A clinical microchip for evaluation of single immune cells reveals high functional heterogeneity in phenotypically similar T cells. *Nat Med* 17(6): 738–743.
13. Lu Y, et al. (2013) High-throughput secretomic analysis of single cells to assess functional cellular heterogeneity. *Anal Chem* 85(4):2548–2556.

14. Shi Q, et al. (2012) Single-cell proteomic chip for profiling intracellular signaling pathways in single tumor cells. *Proc Natl Acad Sci USA* 109(2):419–424.
15. Zhao JL, et al. (2014) Conversion of danger signals into cytokine signals by hematopoietic stem and progenitor cells for regulation of stress-induced hematopoiesis. *Cell Stem Cell* 14(4):445–459.
16. Gordon S, Taylor PR (2005) Monocyte and macrophage heterogeneity. *Nat Rev Immunol* 5(12):953–964.
17. Mosser DM, Edwards JP (2008) Exploring the full spectrum of macrophage activation. *Nat Rev Immunol* 8(12):958–969.
18. Wynn TA, Chawla A, Pollard JW (2013) Macrophage biology in development, homeostasis and disease. *Nature* 496(7446):445–455.
19. Fan J, Malik AB (2003) Toll-like receptor-4 (TLR4) signaling augments chemokine-induced neutrophil migration by modulating cell surface expression of chemokine receptors. *Nat Med* 9(3):315–321.
20. Stow JL, Low PC, Offenhäuser C, Sangermani D (2009) Cytokine secretion in macrophages and other cells: Pathways and mediators. *Immunobiology* 214(7):601–612.
21. Roger T, David J, Glauser MP, Calandra T (2001) MIF regulates innate immune responses through modulation of Toll-like receptor 4. *Nature* 414(6866):920–924.
22. Calandra T, Roger T (2003) Macrophage migration inhibitory factor: A regulator of innate immunity. *Nat Rev Immunol* 3(10):791–800.
23. Mantovani A, et al. (2004) The chemokine system in diverse forms of macrophage activation and polarization. *Trends Immunol* 25(12):677–686.
24. Han Q, et al. (2012) Polyfunctional responses by human T cells result from sequential release of cytokines. *Proc Natl Acad Sci USA* 109(5):1607–1612.
25. Varadarajan N, et al. (2012) Rapid, efficient functional characterization and recovery of HIV-specific human $CD8^+$ T cells using microengraving. *Proc Natl Acad Sci USA* 109(10):3885–3890.
26. Han Q, Bradshaw EM, Nilsson B, Hafler DA, Love JC (2010) Multidimensional analysis of the frequencies and rates of cytokine secretion from single cells by quantitative microengraving. *Lab Chip* 10(11):1391–1400.
27. Geladi P, Kowalski BR (1986) Partial least-squares regression: A tutorial. *Anal Chim Acta* 185:1–17.
28. Ringnér M (2008) What is principal component analysis? *Nat Biotechnol* 26(3):303–304.
29. Newell EW, Sigal N, Bendall SC, Nolan GP, Davis MM (2012) Cytometry by time-of-flight shows combinatorial cytokine expression and virus-specific cell niches within a continuum of $CD8^+$ T cell phenotypes. *Immunity* 36(1):142–152.
30. Amir el-AD, et al. (2013) viSNE enables visualization of high dimensional single-cell data and reveals phenotypic heterogeneity of leukemia. *Nat Biotechnol* 31(6):545–552.
31. Van der Maaten L, Hinton G (2008) Visualizing Data using t-SNE. *J Mach Learn Res* 9(11):2579–2605.
32. Lacey DC, et al. (2012) Defining GM-CSF- and macrophage-CSF-dependent macrophage responses by in vitro models. *J Immunol* 188(11):5752–5765.
33. Kravchenko-Balasha N, Wang J, Remacle F, Levine RD, Heath JR (2014) Glioblastoma cellular architectures are predicted through the characterization of two-cell interactions. *Proc Natl Acad Sci USA* 111(17):6521–6526.
34. Wang J, et al. (2012) Quantitating cell-cell interaction functions with applications to glioblastoma multiforme cancer cells. *Nano Lett* 12(12):6101–6106.
35. Chattopadhyay PK, Gierahn TM, Roederer M, Love JC (2014) Single-cell technologies for monitoring immune systems. *Nat Immunol* 15(2):128–135.
36. Petricoin EF, Zoon KC, Kohn EC, Barrett JC, Liotta LA (2002) Clinical proteomics: Translating benchside promise into bedside reality. *Nat Rev Drug Discov* 1(9):683–695.
37. Altelaar AF, Munoz J, Heck AJ (2013) Next-generation proteomics: Towards an integrative view of proteome dynamics. *Nat Rev Genet* 14(1):35–48.
38. Irish JM, Kotecha N, Nolan GP (2006) Mapping normal and cancer cell signalling networks: Towards single-cell proteomics. *Nat Rev Cancer* 6(2):146–155.